



Electro-oxidation of Ethanol at Gas Diffusion Electrodes A DEMS Study

V. Rao,^{a,z} C. Cremers,^{b,d,*} U. Stimming,^{a,b,*} Lei Cao,^c Shiguo Sun,^c Shiyou Yan,^c
Gongquan Sun,^c and Qin Xin^c

^aDepartment of Physics E19, Technische Universität München, D-85748 Garching, Germany

^bBavarian Center for Applied Energy Research (ZAE Bayern), D-85748 Garching, Germany

^cDalian Institute of Chemical Physics, Direct Alcohol Fuel Cell Group, Liaoning Province, Dalian 116023, China

The ethanol electro-oxidation at gas diffusion electrodes made of different catalysts, Pt/C, PtRu(1:1)/C, and PtSn(7:3)/C, were studied by on-line differential electrochemical mass spectrometry in a wide temperature range (30–90°C) as a function of the anode potential, the fuel concentration, and catalyst loading. The CO₂ current efficiency (CCE) of the ethanol oxidation reaction (EOR) exhibits a maximum at about 0.6 V and decreases rapidly with further increasing potentials. The CCE for the EOR goes down with the increase in concentration of ethanol. CCE for ethanol oxidation reaction shows a strong increase with increasing catalyst loading. The CCE increases with increasing temperature, exceeding 75% at 90°C, 0.1 M ethanol, and 5 mg/cm² Pt catalyst loading. PtSn/C shows high CCE, like Pt/C. But PtRu/C exhibits very small CCE. Of the intermediates, acetaldehyde is quite active for further oxidation. But acetic acid is fairly resistant against further oxidation. Our results indicate that the C–C bond scission observed for the EOR with CCE in excess of 50% has to proceed in parallel with ethanol oxidation to either acetaldehyde or acetic acid, and not sequentially from acetic acid further on, as acetic acid cannot be oxidized any further.
© 2007 The Electrochemical Society. [DOI: 10.1149/1.2777108] All rights reserved.

Manuscript submitted May 22, 2007; revised manuscript received July 9, 2007. Available electronically September 10, 2007.

Direct oxidation fuel cells (DOFCs) have recently attracted major attention, as an alternative to hydrogen fuel cells, mainly due to easier fuel storage and handling. The organic liquids used for DOFCs are much simpler to handle than gaseous hydrogen and also in many cases do not require any new distribution infrastructure as they are already widely available as, e.g., ethanol in its denatured form. The most researched type of DOFC is direct methanol fuel cell, DMFC. The methanol has better kinetics of oxidation on the platinum based catalysts in low temperature range than all other aliphatic alcohols and is also known to oxidize completely to CO₂. This leads to better performance of DMFCs. But some disadvantages of methanol are its toxicity and relatively low boiling point. Also most of the methanol today is produced using natural gas as the base material, which is not a renewable energy resource. Because of these shortcomings ethanol, the next alcohol, is considered to be an option because of being less toxic, high in energy content (ethanol: 8 kWh/kg, methanol: 6 kWh/kg) and its availability from renewable resources.

However, the oxidation of ethanol to CO₂ is much slower in comparison to methanol, as it requires the scission of a C–C bond. So ethanol electro-oxidation is associated with the formation of several unwanted by-products like acetaldehyde and acetic acid. The efficiency of ethanol oxidation can be improved by development of catalysts exhibiting faster kinetics and higher selectivity toward CO₂ as product and by optimizing the oxidation conditions.

Various research groups have made efforts to gain mechanistic understanding of the ethanol oxidation reaction (EOR). The reaction is known to follow a complex multistep mechanism, involving a number of adsorbed reaction intermediates and by-products resulting from incomplete ethanol oxidation.¹ The major adsorbed intermediates were identified as adsorbed CO and R_{ads} and R-C_{ads} hydrocarbon residues, whereas acetaldehyde and acetic acid have been detected as the main by-products using differential electrochemical mass spectrometry (DEMS),² infrared spectroscopy,³ or chromatography.⁴ Wang et al. studied the relative product distribution for the EOR in a polymer electrolyte fuel cell operating with ethanol as the anode feed using on-line mass spectrometry in the temperature range between 150 and 190°C and water: ethanol molar

ratios between 5 and 2.⁵ They reported acetaldehyde as the main reaction product, whereas CO₂ only a minor product, without many differences in the product selectivities on Pt–Ru and Pt-black catalysts. Using chromatographic techniques, Hitmi et al. found that at low ethanol concentrations the main product is acetic acid, whereas acetaldehyde is the major product at high concentration (>0.1 M) during ethanol oxidation on polycrystalline Pt at 10°C. Arico et al. investigated the electrochemical oxidation of ethanol in a liquid-feed solid polymer electrolyte fuel cell operating at 145°C, 4 atm anode pressure, 5.5 atm cathode pressure, and 1 M ethanol. Under these conditions, using 2 mg/cm² 60% PtRu/C as anode catalyst, high selectivity toward CO₂ formation (95%) was reported.⁶ Fujiwara et al. studied ethanol oxidation for selectivity to CO₂ vs acetaldehyde on electrodeposited Pt and PtRu electrodes using model electrochemical cell DEMS and reported that Ru addition helps in formation of more CO₂ and less acetaldehyde.²

Camara and Iwasita investigated the effects of ethanol concentration on the yields of CO₂, acetic acid, and acetaldehyde as electro-oxidation products on the polycrystalline Pt electrode using Fourier transform-infrared (FTIR) spectroscopy. They found acetic acid as a major product at low ethanol concentrations, and CO₂ being produced to a minor extent. With increasing ethanol concentrations, the pathway producing acetaldehyde becomes dominant.⁷ Wang et al. studied the product distribution for EOR systematically as a function of temperature and concentration in a model DEMS for supported platinum catalyst (Pt/C).⁸ Very low CO₂ formation was reported for EOR at their working conditions. They investigated Pt/C, Pt₃Sn/C, and PtRu/C catalysts for EOR and reported that the addition of Sn and Ru increases the faradaic activity without any increase in the CO₂ current efficiency which was reported to be 1% in all cases.⁹ Lamy's group at the University of Poitiers has published a number of papers about the PtSn based catalyst for EOR.^{10–12} Sn is proposed to activate adsorbed water at lower potential than Pt, leading to higher activity.^{13,14} They studied the product distribution of EOR in a fuel cell with high performance liquid chromatography (HPLC) and reported 20% CO₂ formation for Pt/C catalyst, which reduced to around 7% in the case of Pt–Sn and Pt–Sn–Ru based catalyst. The last two catalysts were reported to favor acetic acid as the final product.¹⁵

However, as discussed above, the results about the mechanism of ethanol oxidation vary widely depending on several parameters like oxidation in a model electrochemical cell or at a fuel cell membrane electrode assembly (MEA), temperature, concentration, etc. Also

* Electrochemical Society Active Member.

^d Present address: Fraunhofer Institute for Chemical Technology, Division of Applied Electrochemistry, D-76327 Pfintzal, Germany.

^z E-mail: vrao@ph.tum.de

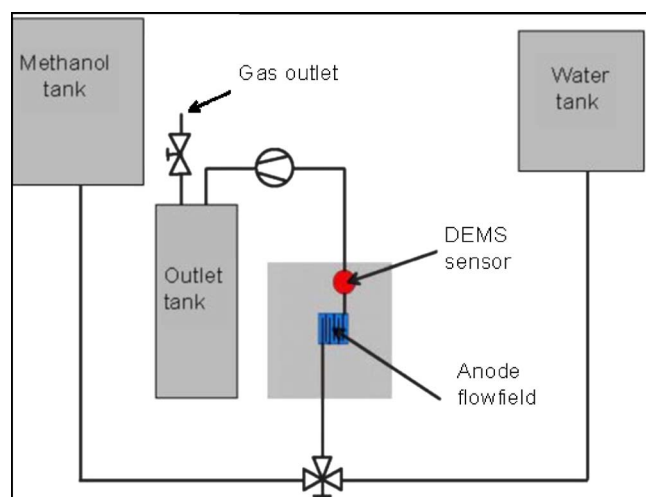


Figure 1. (Color online) Schematics of the fuel cell DEMS setup.

most of the systematic studies about the ethanol oxidation reaction were done at a model electrode (single crystal or thin layer electrode in electrochemical cells) and may not directly apply to actual fuel cell conditions.

It is our aim in this paper to illustrate the mechanism of ethanol oxidation under real fuel cell conditions by investigating systematically the effect of various parameters such as temperature, concentration, potential, catalyst layer thickness, active area in a catalyst layer, and intrinsic nature of the catalyst on the CO_2 current efficiency for EOR using an in situ technique of fuel cell DEMS. We propose that the C–C bond cleavage rate is not only affected by the intrinsic nature of catalyst, but also similarly or even more strongly affected by the above-mentioned anodic oxidation conditions.

Experimental

Membrane electrode assembly.—40% Pt/C, unsupported Pt (Alpha Aesar), 20% Pt:Ru(1:1)/C(E-TEK) and 20% Pt:Sn(7:3)/C are used as anode catalysts for different sets of experiments; 40% Pt/C is used as the cathode catalyst. The metal catalyst loading on the cathode side is kept high at around 4 mg/cm^2 . In order to make a membrane electrode assembly, an emulsion of catalyst powder, liquid Nafion and isopropanol is treated in an ultrasonicator. The ink prepared in this way is sprayed onto the porous carbon backing layers (Toray paper from E-TEK, TGPH 060, no wet proofing), held at 110°C . The 1.2 cm^2 patches of the catalyst sprayed on Toray paper were then cut and hot pressed with the N-117 Nafion membrane in between, at 140°C for 5 min. The MEA sandwich is hot pressed at a pressure of 826 N/cm^2 .

Experimental setup.—The fuel cell consisted of two stainless steel plates with integrated serpentine flow field. Six threaded studs and nuts held the two plates together. The fuel cell can be operated in both modes of half cell and full cell. Generally during the investigation of the anode it is used as a half cell. Cathode with high Pt loading (4 mg/cm^2) and continuous hydrogen flow works as counter and reference both. Potential of the cathode is assumed to be the same as of the reversible hydrogen electrode (RHE). All potentials are reported in reference to this.

The anode flow system is comprised of a tank filled with alcohol solution and a tank filled with water. These tanks are connected via heated tubes with the three-way valve at the fuel cell inlet (cf. Fig. 1). The alcohol solution and the Millipore water are always deaerated with argon. A liquid pump between the cell outlet and exit tank controls the flow of alcohol solution and water through the cell. The flow rate is generally kept at 5 mL/min in all experiments, unless otherwise mentioned. To avoid the gas bubble formation due to the

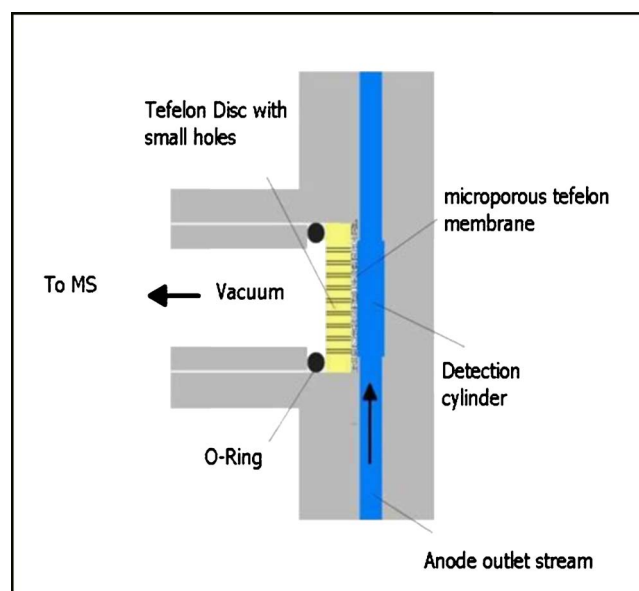


Figure 2. (Color online) Design of MS sensor.

large gas production and low solubility of CO_2 at elevated temperature, the anode flow system is pressurized at 4 bars (abs) pressure. The cathode pressure is kept at 2 bar (abs) to limit the crossover of H_2 to the anode side. The hydrogen diffusing from the cathode side to the anode side gets oxidized at the anode and thus interferes with the measurement of the anodic currents. So it is important to keep the amount of hydrogen diffusing to the anode side rather small. The permeation of alcohol to the cathode side does not affect the potential of the cathode (which is also a reference electrode).

At the outlet channel of the anode compartment, the DEMS sensor is positioned. It consists of a cylindrical detection volume with a diameter of 7 mm and a height of 2 mm through which anode outlet flow passes (cf. Fig. 2). This volume is separated from the vacuum system of the mass spectrometer by a microporous Teflon membrane (Schleicher & Schuell, TE30) with a pore size of $0.02 \mu\text{m}$ and a thickness of $110 \mu\text{m}$. The membrane is supported by a 2 mm thick Teflon disk having few 0.1 mm holes. A Balzer Prisma QMS 200 mass spectrometer and a potentiostat designed by AGEF are used together with a computerized data acquisition system. Details about this fuel cell DEMS setup have been published earlier.¹⁶

Experimental strategies.—It is known that the different oxidation products of ethanol are carbon dioxide, acetaldehyde, and acetic acid. Out of them, only the first two are volatile enough to be monitored by DEMS. However, the problem is that both CO_2 and CH_3CHO have the same molecular mass of 44 g/mol and thus overlapping molecular ion peak signal at $m/z = 44$. So to monitor both together is not possible at $m/z = 44$. One way of solving this problem is by using deuterated ethanol ($\text{CD}_3\text{CH}_2\text{OH}$), an approach utilized by Fujiwara et al.,² for determining the product yield ratio between carbon dioxide and acetaldehyde. But the high cost of deuterated ethanol precludes its use for extensive experiments. Another approach is to monitor them as their major fragments. For CO_2 the $m/z = 22$ corresponding to doubly ionized CO_2^{2+} molecular ions can be used, which has been reported by Wang et al.⁸ Similarly for acetaldehyde the most prominent fragment COH^+ at $m/z = 29$ can be used.

Thus $m/z = 22$ and 29 signals were monitored during ethanol oxidation for observing CO_2 and CH_3CHO formation. The calibration of DEMS for CO_2 is performed with potentiostatic bulk CO oxidation. Figure 3 shows a good signal for $m/z = 22$, although the signal quality is not as good as for $m/z = 44$, as the $m/z = 22$ ion current is about a factor of 30 smaller.

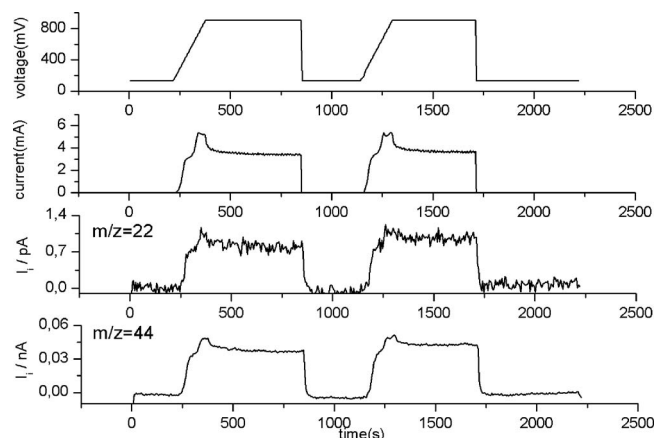


Figure 3. This figure shows voltage, bulk CO oxidation current, and $m/z = 22$ and 44 signal as a function of time.

The calibration constant is calculated using the formula

$$K_F^* = \frac{2I_{MS}}{I_F} \quad [1]$$

where I_{MS} is the steady state ion current for $m/z = 22$, and I_F is the corresponding faradaic current.

In order to measure the current efficiency of CO_2 formation for ethanol oxidation reaction, potentiostatic oxidation is performed at various potentials, temperatures, and concentrations of ethanol. Calibration constants are obtained for all temperatures separately. Then the CO_2 current efficiency for ethanol oxidation reaction can be calculated using the formula

$$\eta (\text{CO}_2 \text{ current efficiency}) = \frac{6I_{MS}}{I_F K_F^*} \quad [2]$$

where I_{MS} is the steady state ion current for $m/z = 22$ for ethanol oxidation, and I_F is the corresponding faradaic current. I_{MS} and I_F values were measured 6–10 min after the potential pulse is taken for calculating CO_2 current efficiency. The error in determination of CO_2 current efficiency is determined by the $m/z = 22$ signal quality. This could give an error of around ± 10 –15%.

Results and Discussion

CO_2 current efficiency as a function of potential and temperature.— Figure 4 shows that the CO_2 current efficiency strongly depends on potential and temperature. The increase in the CO_2 current efficiency with temperature can be explained by the fact that the kinetics of the C–C bond breaking will be accelerated at higher temperatures. The decrease in CO_2 current efficiency after 0.6 V is a bit of a surprising result. However, it is expected that at potentials > 0.8 V the Pt surface is significantly covered by chemisorbed oxygen, which may hinder the complete oxidation of ethanol, but could support formation of various oxidation by-products like acetaldehyde and acetic acid.⁸ It was also found that the formation of acetaldehyde is more favored at high potentials, as can be seen in Fig. 5; $m/z = 29$ is assigned to the major acetaldehyde fragment COH^+ . In Fig. 5 the mass spectrometer cyclic voltammogram (MSCV) of $m/z = 22$ has a peak at around 850 mV and after that it declines. On the contrary, $m/z = 29$ (acetaldehyde) follows the faradaic current, as it becomes flatter at higher (> 1 V) potentials, with no decrease in $m/z = 29$ ion current. Acetaldehyde formation depends strongly on the concentration and temperature as well. At higher temperature and lower concentration less acetaldehyde is formed as can be seen in Fig. 6 and 7.

The $m/z = 15$ corresponds to the CH_3^+ ion which is a fragment of methane. However, acetaldehyde also has a fragment at $m/z = 15$

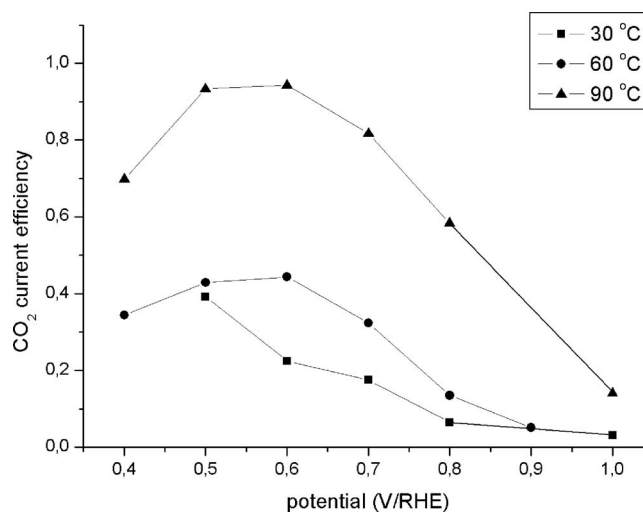


Figure 4. CO_2 current efficiency vs potential for different temperatures. Measurement is done in a fuel cell MEA. Anode: 40% Pt/C, 5 mg/cm^2 metal loading. Anolyte: 0.1 M ethanol.

(rel. abundance 40%). Formation of methane is reported to occur by the cathodic reduction of the adsorbed species, formed by the dehydrogenation of ethanol on catalysts surfaces.^{8,17} In Fig. 5, the m/z

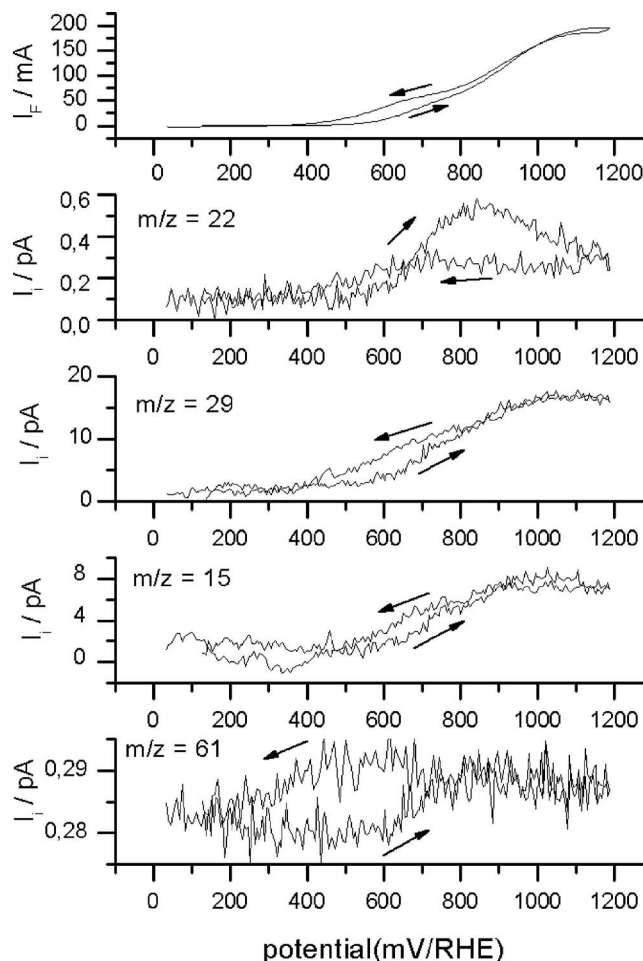


Figure 5. This figure shows CV and MSCV for $m/z = 22, 29, 15,$ and 61. The anode feed is 1 M EtOH at 5 mL/min at 30°C. Scan rate is 1 mV/s .

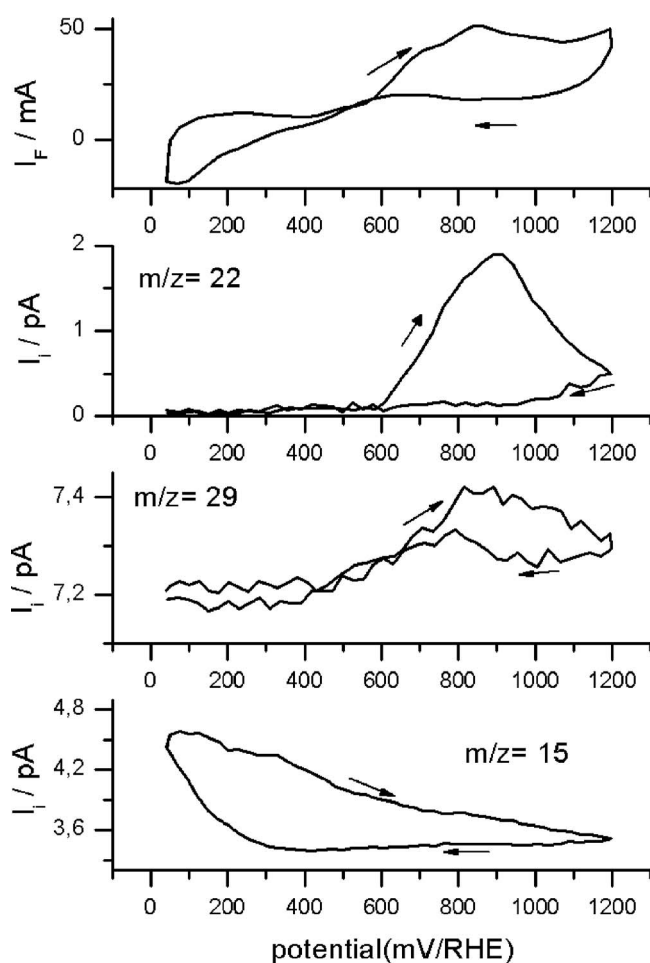


Figure 6. This figure shows CV and MSCV for $m/z = 22, 29,$ and 15 . The anode feed is 0.1 M EtOH at 5 mL/min at 30°C . Scan rate is 5 mV/s.

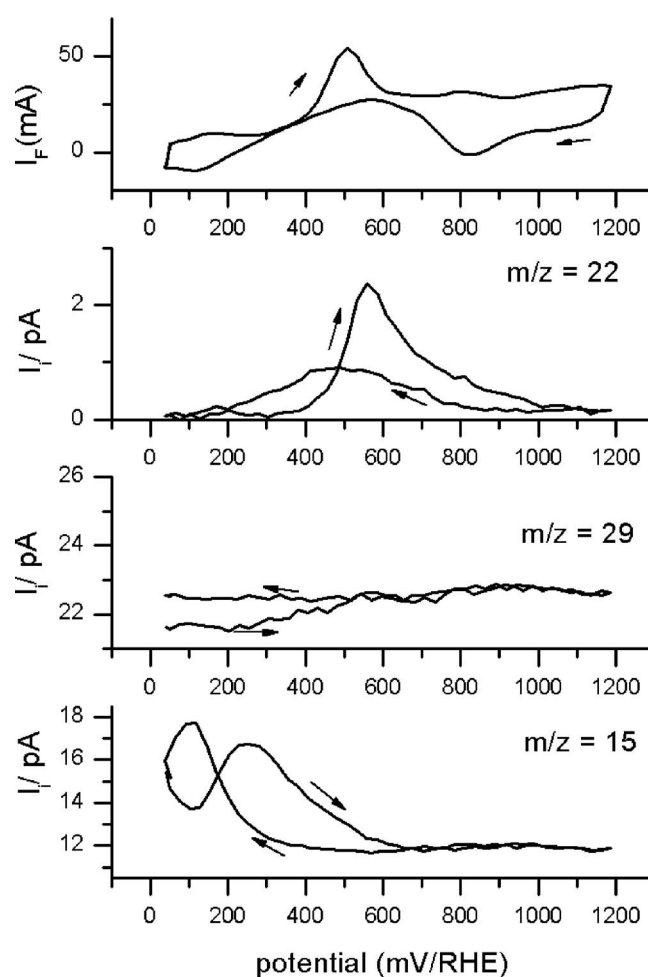


Figure 7. This figure shows CV and MSCV for $m/z = 22, 29,$ and 15 . The anode feed is 0.01 M EtOH at 5 mL/min at 90°C . Scan rate is 5 mV/s.

$m/z = 15$ signal rises with the potential on the positive side and almost follows the $m/z = 29$ (CH_3CHO) signal, as acetaldehyde is the main source of CH_3^+ fragment in potential range >0.4 V. Cathodic production of methane is overshadowed by the CH_3CHO , which is a major product at 1 M EtOH concentrations and low temperature. But at lower concentration of 0.1 M EtOH, with high CO_2 current efficiency (40% at 30°C and 0.5 V), CH_3CHO seems to be a minority product, as there is no rise in $m/z = 15$ signal in the positive potential range (cf. Fig. 6). At 0.01 M EtOH and at 90°C there is no formation of acetaldehyde as can be seen in both $m/z = 15$ and $m/z = 29$ signals (cf. Fig. 7). In both cases cathodic methane is formed in the potential range <0.4 V as can be inferred from the rising signals of $m/z = 15$ in Fig. 6 and 7. The $m/z = 61$ is a fragment (100% rel. abundance) of ethyl acetate, which provides an indirect way of monitoring acetic acid. Though the acidic environment of the catalyst layer enhances the kinetics of ester formation it also enhances the kinetics of ester cleavage so that it may be assumed that the ester is only present in its equilibrium concentration which will be low considering the large excess of water present. Furthermore, the boiling point of the ester is also rather high; at 77°C only a weak signal will be found in the DEMS so that it mostly will be used as an indication of acid formation and not to quantify the amount of acid that gets formed. The formation of ethyl acetate is through the esterification reaction between the acetic acid (formed as a by-product of ethanol, oxidation) and unreacted ethanol, possibly catalyzed by the acids; $m/z = 61$ in Fig. 5 shows that

the onset of the formation of ethyl acetate is around 600 mV and after that signal saturates at higher potentials. In the negative scan it shows a peak at around 500 mV.

The CO_2 current efficiency for ethanol oxidation, which is found in our fuel cell DEMS measurements, is significantly (about an order of magnitude) higher than what has been reported in model electrochemical systems with thin catalyst layers or polycrystalline platinum electrodes, as measured by Wang et al.⁸ using DEMS, by Camara and Iwasita⁷ using FTIR spectra and by Vigier et al.¹⁴ using HPLC. It is likely because of a thicker catalyst layer (>100 μm with 5 mg/cm² metal loading using 40% Pt/C, in our case), where the desorbed and dissolved intermediates stay a longer time in proximity to the catalyst allowing for readsorption and thus resulting in a more complete oxidation of the ethanol. The thickness of the catalyst layer obviously plays an important role in the formation of the final by-products, as thin layers seem to produce more acetaldehyde. The effect of the catalyst loading and thus catalyst layer thickness on the CO_2 current efficiency for ethanol oxidation is discussed later in this article.

CO₂ current efficiency as a function of concentration.— The CO_2 current efficiency decreases with increasing concentrations of ethanol as can be seen in Fig. 8. This tendency is more clearly visible in lower potential range. In high potential range this trend is disturbed because of other effects coming into play. This result of cathode current efficiency (CCE) dependence on ethanol concentration agrees with the findings of DEMS^{8,18} and FTIR spectroscopy⁷

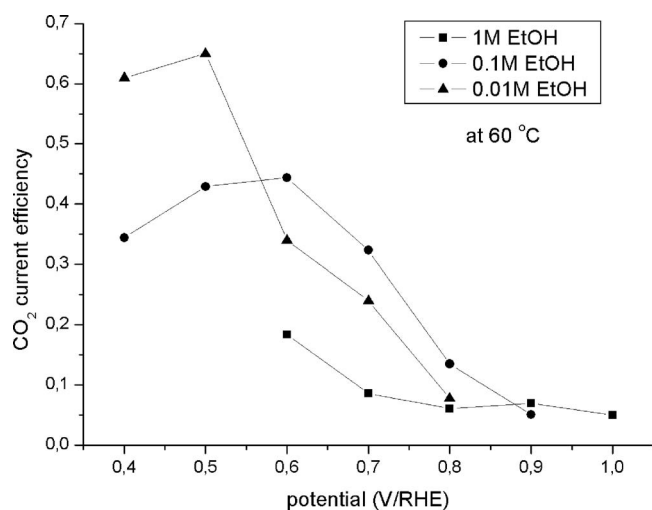


Figure 8. CO₂ current efficiency vs potential for different ethanol concentrations, at 60 °C.

experiments on ethanol oxidation. The similar tendency of CO₂ current efficiency variation with increasing concentration has also been reported for methanol oxidation reaction.^{19,20}

As can be seen in Fig. 9, the CO₂ production passes through a maximum with increase in EtOH concentration, which is reasonable because as the concentration of EtOH increases, the partial reactions like formation of acetaldehyde become dominant. This observation agrees well with the results of Camara and Iwasita,⁷ who reported that the CO₂ production passes through a maximum at 0.025 M C₂H₅OH and then decreases, for their polycrystalline platinum electrode. In our case this optimum concentration is around 0.1 M. This difference is explained by the difference in the electrode structure, which in our case is a thick layer made up of nanoparticle catalyst.

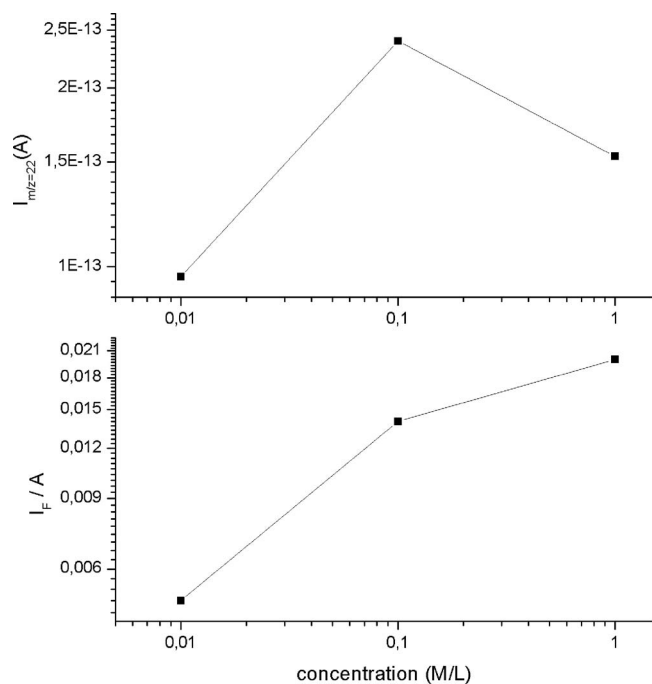


Figure 9. The $m/z = 22$ ion current and faradaic current vs concentration on log scale. Temperature: 30 °C, potential of oxidation: 0.6 V. Catalyst: 40% Pt/C and loading: 5 mg/cm².

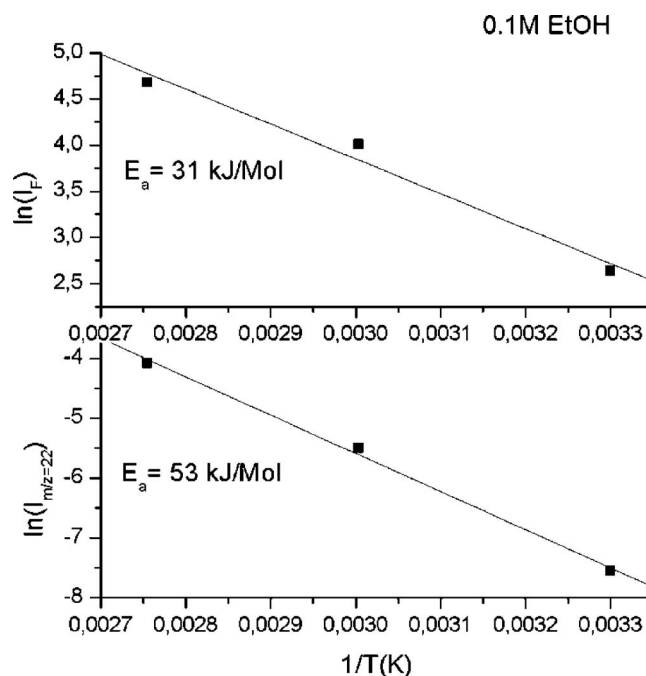


Figure 10. Arrhenius plots with 0.1 M EtOH and at 0.6 V RHE. Catalyst used is 40% Pt/C and loading is 5 mg/cm².

Activation energy calculation.— From the linear slopes of the Arrhenius plots in Fig. 10, the averaged apparent activation energy is determined for overall ethanol electro-oxidation reaction and for partial reaction of the formation of the product CO₂. The apparent activation energy calculated from the faradaic currents for ethanol oxidation in the temperature range 30–90 °C (with 0.1 M EtOH and at 0.6 V RHE) over the 40% Pt/C catalyst, is 31 kJ/mol, agrees quite well with the literature. The activation energy for CO₂ formation was calculated after correcting the $m/z = 22$ ion current for temperature effects of MS, and is 53 kJ/mol. This does not agree with the apparent activation energy for CO₂ formation reported by Wang et al.,⁸ which is 20 kJ/mol. But Wang et al. used the overall charge from CV in ethanol in potential range 0–1.2 V/RHE, for calculating apparent activation energy instead of potentiostatic bulk oxidation currents at 0.6 V/RHE, as in our case. In our experiments it was found that the CCE depends strongly on the potential of oxidation. So this difference in the protocol of activation energy calculation may explain the difference in the values of apparent activation energy for CO₂ formation.

Effect of catalyst layer thickness or catalyst loading.— The effect of catalyst loading, and thus the catalyst layer thickness, on the CO₂ current efficiency for ethanol oxidation reaction is very important to understand for evaluating different catalysts under fuel cell conditions. But this effect has more to do with the physical parameters of catalyst layer and flow conditions than the activity of the catalyst towards ethanol oxidation reaction. The porosity, pore size distribution, reactant flow rate, and residence time determine the product distribution particularly if partially oxidized intermediates can desorb from the catalyst and be reabsorbed at the same or a different active surface site. For low catalyst loading cases, negligible CO₂ current efficiency was observed at 30 °C. This result agrees well with the literature.^{7,8,14} With our fuel cell DEMS system operating at 3 bar overpressure it is also possible to measure CO₂ current efficiency at higher temperatures as well and it was found to be increasing with increasing catalyst loading and almost saturating at a level of 80%, at 90 °C, with a catalyst loading of 8 mg cm⁻², (cf. Fig. 11a and b).

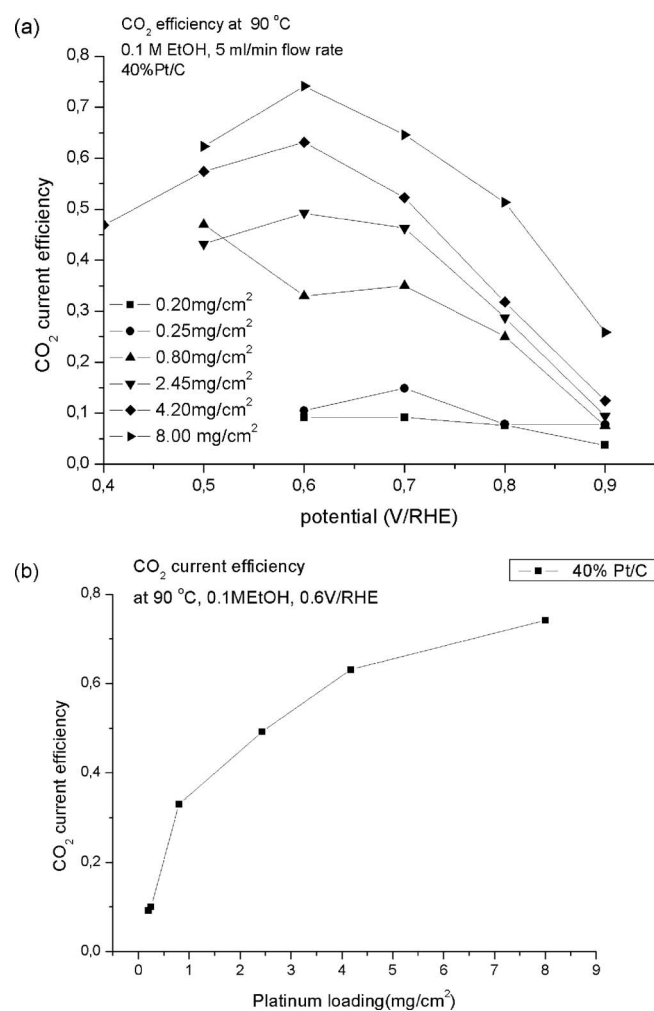


Figure 11. (a) CO₂ current efficiency vs potential for different catalyst loadings, at 90 °C. (b) Variation of CCE as a function of metal loading at oxidation potential of 0.6 V/RHE. Anode feed is 0.1 M EtOH with 5 mL/min flow speed. Catalyst used is 40% Pt/C.

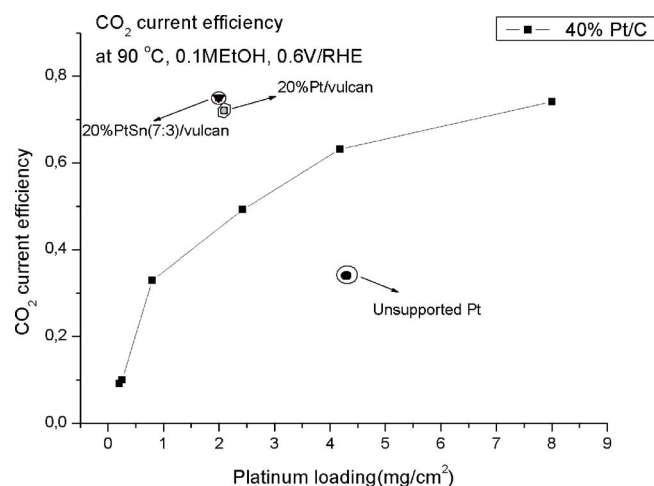


Figure 12. Dependence of CCE on the platinum metal loading in an anode catalyst layer. CCE values for unsupported Pt, 20% Pt/C, and 20% PtSn/C are also shown. Potential: 0.6 V/RHE. Anode feed is 0.1 M EtOH.

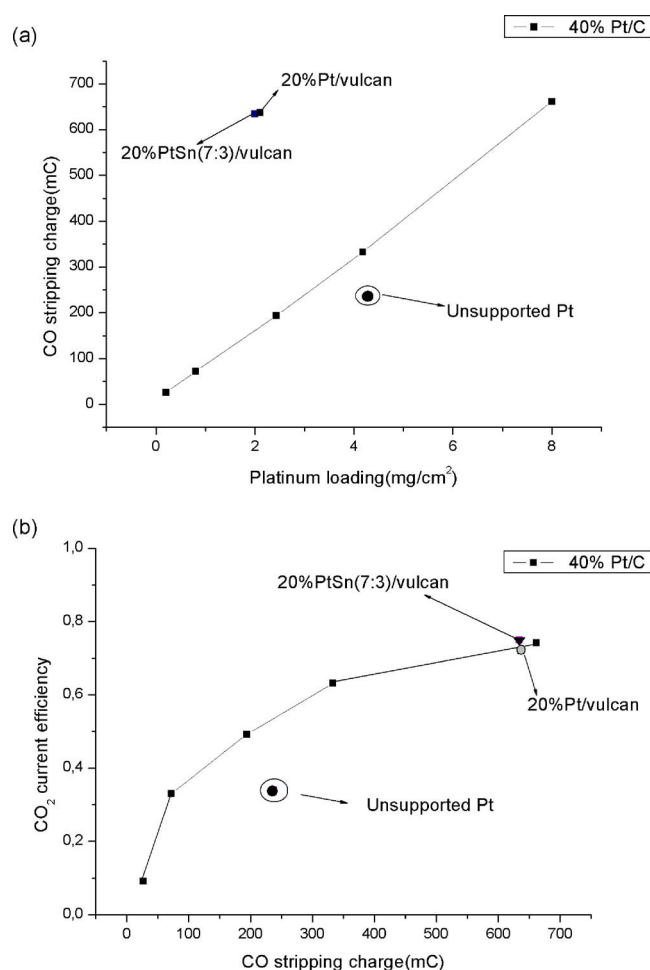


Figure 13. (a) CO stripping charge variation with the platinum metal loading in catalyst layers. (b) Dependence of CCE on the CO stripping charge for anode catalyst layer.

Different catalysts show different CCE even with the same metal loading.— The CCE for a catalyst increases with increasing catalyst loading, as has been discussed earlier for the case of 40% Pt/C. But platinum loading itself does not seem to be the determinant for CCE as it was found that other catalysts like unsupported Pt and 20% Pt/C do not follow the same dependence on catalyst loading like 40% Pt/C (cf. Fig. 12). The reason behind this discrepancy is the difference in the electrochemically active surface area (EASA). The EASA is the area which is available for initial adsorption/oxidation of ethanol and further readsorption of the intermediates of EOR. The next section deals with the effect of the EASA on the CCE. The CCE data for 20% PtSn/C catalyst are also shown in Fig. 12.

Effect of electrochemically active surface area available in the catalyst layer on the CCE.— For the same catalyst the CCE vs metal catalyst loading follows a sigmoidal curve. But these curves are different for catalysts with different metal percentages on carbon support or unsupported catalyst. To understand this, the EASA was measured for each catalyst layer and metal loading. EASA was measured by standard CO stripping technique. Figure 13a shows the CO stripping charge vs platinum loading, which is quite linear with the metal loading up to 8 mg/cm² for 40% Pt/C. EASA is directly proportional to the CO stripping charge with a conversion factor of 420 $\mu\text{C}/\text{cm}^2$. The catalysts 20% PtSn/C, 20% Pt/C, and unsupported Pt are also indicated in Fig. 13a. As expected, 20% PtSn/C and 20% Pt/C have better dispersion and higher EASA than 40% Pt/C for the same Pt loading. Similarly unsupported Pt has lower EASA than

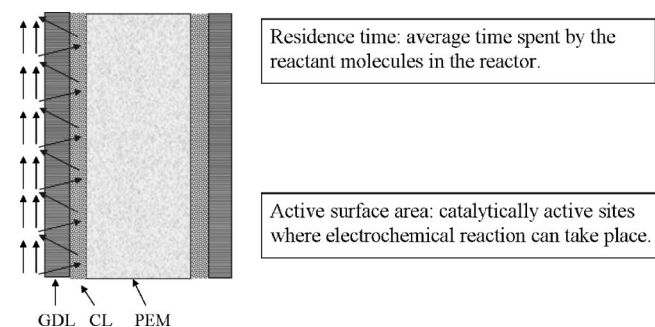


Figure 14. This figure illustrates the flow and diffusion conditions in a fuel cell MEA (membrane electrode assembly). The convective flow takes place in a flow field channel. Diffusion is the dominant transport mechanism in GDL and CL.

40% Pt/C for similar Pt loading which is also as expected. Figure 13b shows the CCE vs the CO stripping charge (EASA). In this figure the 20% PtSn/C and 20% Pt/C seem to follow the same curve as 40% Pt/C but not so the unsupported Pt sample. This result is probably explainable by invoking the concept of a chemical reactor. Quite reasonably the fuel cell electrode can be assumed to work as a chemical reactor, since fuel cell electrodes also have an active area and reactants flowing in (cf. Fig. 14). Then in such a case the product distribution is dictated by the residence time and active area available for the reaction to occur. This could explain the lower CCE for unsupported catalyst for similar EASA. The unsupported catalyst will have lower residence time because of the thin layer for similar metal loading and EASA, as there is no low density carbon support in the catalyst layer. This lower residence time under similar conditions could give rise to lower CCE. Wang et al.⁸ also reported an increase in CCE for EOR when they changed their electrode from polycrystalline Pt to catalyst layer made from a nanoparticle Pt powder in their thin layer flow cell DEMS. This is in agreement with our results as the catalyst layer made from nanoparticle Pt powder would have higher active area in comparison to smooth polycrystalline Pt electrode. The catalyst 20% PtSn/C exhibits similar CCE as the 20% Pt/C and 40% Pt/C at similar EASA. This is a rather unexpected result as addition of Sn to platinum should result in some changes in the catalytic properties of platinum. But on the other hand Sn, which is known to act as an oxygen/oxygenated species provider for EOR, unlike Ru, is not known to adsorb carbonaceous species.²¹ Thus it might be proposed that Sn in PtSn bifunctional catalyst acts only as a oxygen provider and does not alter the adsorption properties of Pt itself. This could be a possible explanation for PtSn/C catalyst exhibiting similar CCE as Pt/C catalyst.

CCE dependence on anolyte flow rate.— The CCE depends strongly on the thickness of the catalyst layer and the available electrochemical active area in the catalyst layer. The thickness of the catalyst layer would control the residence time of the ethanol molecules in the catalyst layers. Another possible way to change the residence time of the reactants is by changing their flow rates. To understand this behavior, the effect of anolyte flow rate on CCE for EOR was investigated. Figure 15 shows the variation of the CCE with the anolyte flow rate. The fuel cell MEA has convection and diffusion as the mechanisms for reactant transport to the catalyst layer. By changing the flow rate mostly convection in the flow field channel will be changed, with diffusion rates in gas diffusion layer (GDL) and catalyst layer (CL) remaining the same. Diffusion is the dominant mechanism of reactant transport in the GDL and CL. This might explain that changing the flow rate by a factor of 30 changes the CCE only by 20%.

Dependence of CCE on the intrinsic nature of catalyst.— It was found that CCE depends strongly on the physical properties of the catalyst layer. But still one of the most important determinants

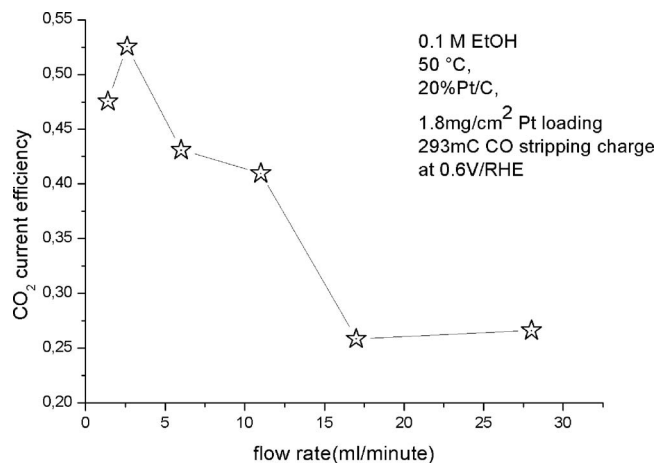


Figure 15. CCE variation as a function of anolyte flow rate.

for the CCE is the intrinsic nature of the catalyst. In our investigation, the unsupported Pt, 20% PtSn(7:3)/C, and 20% PtRu(1:1)/C catalysts were studied for EOR. It was found that under similar working conditions, the CCE for PtSn and Pt catalysts is high. But

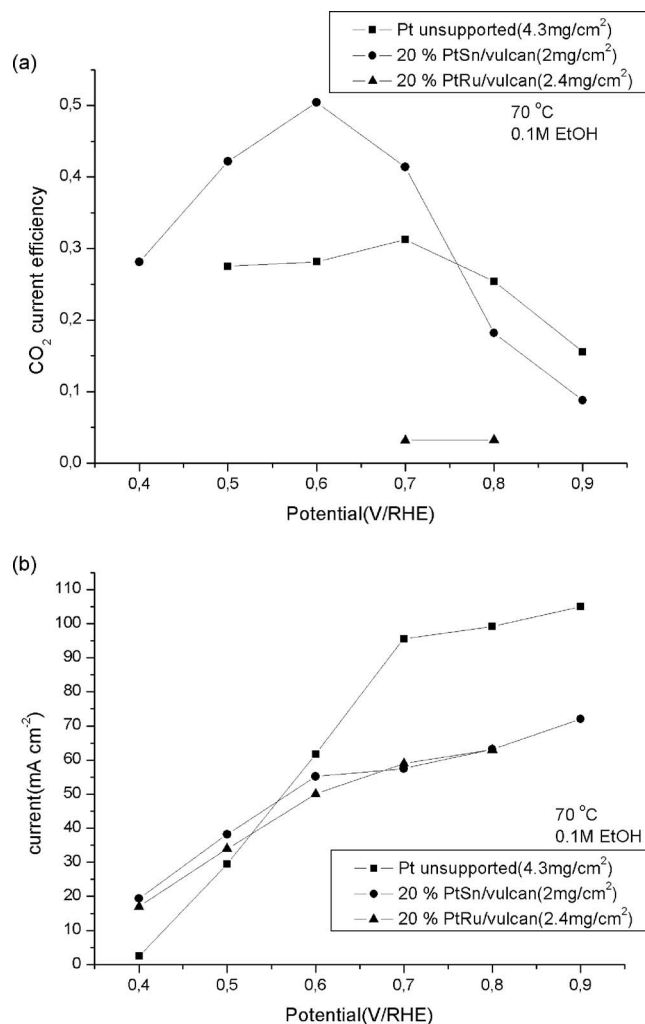


Figure 16. (a) CCE as a function of potential for unsupported Pt, 20% PtSn(7:3)/C, and 20% PtRu(1:1)/C, (b) faradaic currents as a function of potential for all three catalysts.

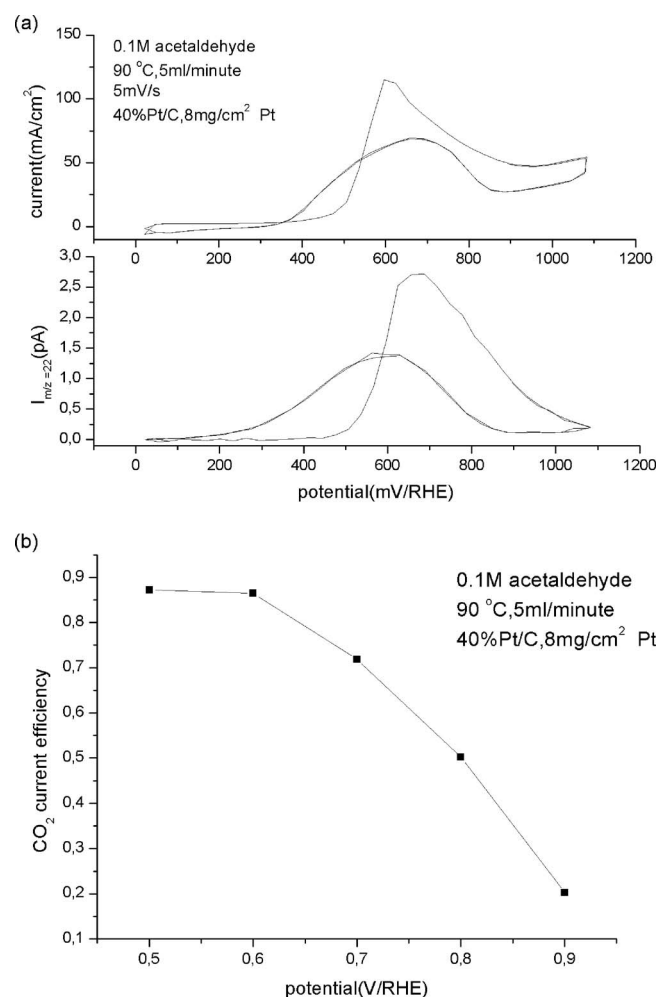


Figure 17. (a) CV and MSCV for 0.1 M acetaldehyde at 90°C, (b) CCE for acetaldehyde oxidation reaction as a function of potential. Catalyst used is 40% Pt/C with 8 mg/cm² metal catalyst loading.

PtRu catalyst gave completely different results (cf. Fig. 16a). Although the faradaic current was comparable to PtSn catalyst, the CCE was found to be very low in comparison (cf. Fig. 16b). In the literature similar results have been reported for a rather similar compound, ethylene glycol (EG), which also contains one C–C bond. De Lima et al.²² studied ethylene glycol electro-oxidation on PtRu catalysts with different Ru contents and reported that more Ru-rich catalysts tend to form more partially oxidized by-products than CO₂. The oxide covered Ru sites on one hand help in oxidation of CO-like adsorbed species but on the other hand hinders the dissociative adsorption of EG and thus promotes the partial oxidation reaction. This seems to apply to EOR as well, as our catalyst PtRu(1:1) demonstrates very low CCE as can be seen in Fig. 16a. For the same electrochemical active area in the catalyst layer 20%PtSn(7:3)/C catalyst exhibits similar CCE as pure Pt based catalyst as has been discussed earlier. This result does not agree with the results reported in Ref. 15. In this paper Rousseau et al.¹⁵ reported that addition of Sn to Pt catalyst brings down the CO₂ yield in ethanol oxidation reaction, although Wang et al.⁹ reported similar CO₂ current efficiency for Pt/C and Pt₃Sn/C catalysts for ethanol oxidation reaction, which agrees with our results. The actual reason behind these differences related to CO₂ current efficiency of PtSn based catalysts for EOR is not yet clear.

Direct oxidation of acetaldehyde and acetic acid.— Acetaldehyde oxidation was investigated in the fuel cell to determine the

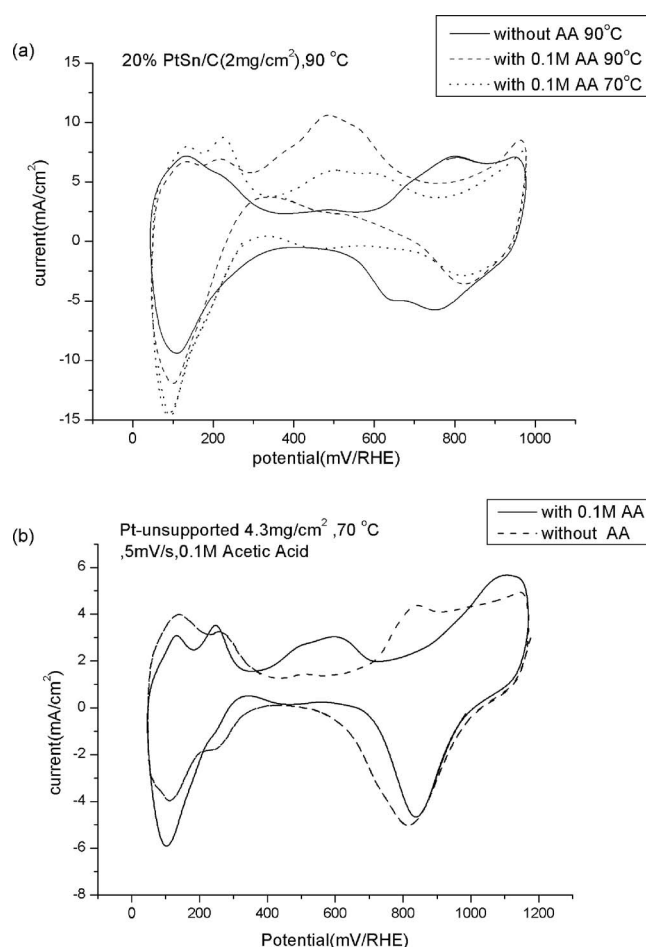


Figure 18. (a) CV in 0.1 M acetic acid at 70°C and 90°C for 20% PtSn/C (2 mg/cm²) as catalyst, (b) CV in 0.1 M acetic acid at 70°C for unsupported Pt (4.3 mg/cm²).

nature and quantity of products of oxidation. The experiment showed that acetaldehyde is quite active for further oxidation as the faradaic currents were comparable to ethanol oxidation reaction in similar conditions and with same catalyst, namely Pt/C. The CCE in acetaldehyde oxidation reaction is around 86% at 0.6 V, which is also similar to CCE for ethanol oxidation reaction (cf. Fig. 17). These results showed that if acetaldehyde is formed as an intermediate in ethanol oxidation reaction, it is still quite active for further oxidation.

Similar experiments of direct oxidation were performed with 0.1 M acetic acid also to check if it is possible to oxidize it further and what could be the final products of oxidation reaction. Direct oxidation of acetic acid in fuel cell with Pt/C and PtSn/C both showed almost negligible faradaic currents in comparison to ethanol oxidation. Figure 18 shows the cyclic voltammograms in 0.1 M acetic acid for PtSn/C and unsupported Pt catalysts. The CV with acetic acid solution as anolyte in the case of both catalysts shows a peak around 500 mV. This peak seems to be because of oxidation of some CO-like species. The peaks in hydrogen region in the CV are not much suppressed, which indicate a low coverage of CO-like species. After this peak at around 700 mV, the currents in acetic acid CV are similar to the base CV in deionized water. The faradaic currents in acetic acid CV are further compared with the currents in CV with ethanol as anolyte in Fig. 19. The faradaic currents for acetic acid oxidation reaction are almost negligible in comparison to ethanol oxidation reaction. This indicates that acetic acid is a final product of ethanol oxidation reaction, which is not oxidizable any further.

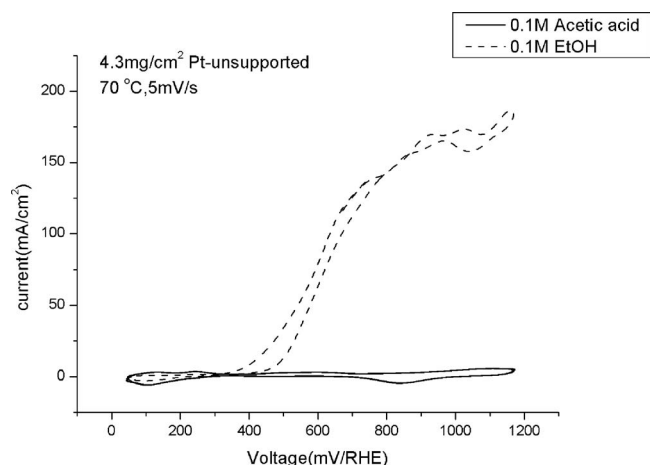


Figure 19. CV in 0.1 M acetic acid and 0.1 M ethanol at 70°C for unsupported Pt (4.3 mg/cm²).

Ethanol oxidation reaction mechanism in fuel cell conditions.—

The CO₂ current efficiency for ethanol oxidation reaction is influenced by many factors related to fuel cell operation. The main intermediates/by-products of ethanol oxidation reaction are acetaldehyde and acetic acid. To understand if acetaldehyde and acetic acid can be oxidized further, separate experiments were performed with acetaldehyde and acetic acid as the anolyte. Acetaldehyde oxidizes readily with very high CCE. But acetic acid is found to be quite resistant to oxidation on Pt and PtSn based catalysts. So acetic acid seems to be the final product. Taking into account these results, we can present the ethanol oxidation reaction mechanism in fuel cell conditions, as shown in Fig. 20. The CCE values indicated in Fig. 20 are for an anode metal catalyst loading of 8 mg/cm² using 40% Pt/C and 90°C and 0.1 M ethanol concentration. Starting from ethanol, there are two pathways towards the formation of CO₂. The first is by direct dissociative adsorption of ethanol and then further oxidation of these adsorbed species. Existence of this pathway for EOR on Pt based catalysts has been reported in the literature.^{8,17} The second is by formation of acetaldehyde and then dissociative adsorption of acetaldehyde, and then further oxidation of the adsorbed species thus formed. These two pathways together result in an overall CO₂ current efficiency of 75%. The remaining faradaic current results either from a two-electron transfer process of partial oxidation of ethanol to an amount of acetaldehyde that leaves the cell, or from a four-electron transfer process of partial oxidation of ethanol to acetic

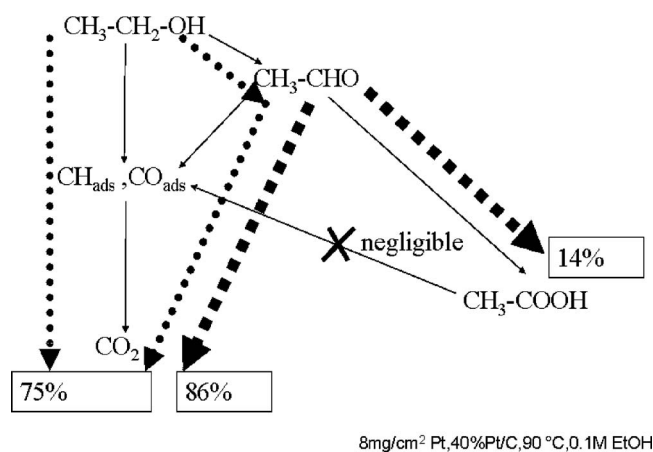


Figure 20. Ethanol oxidation reaction mechanism scheme in fuel cell conditions.

acid via acetaldehyde. Since acetic acid is difficult to oxidize any further, it flows out quantitatively as a final by-product. Figure 20 also shows the CCE for acetaldehyde as the starting molecule. In the fuel cell conditions acetaldehyde oxidation reaction results in 86% CO₂ current efficiency. The rest of the faradaic current results from acetic acid formation.

Conclusion

Ethanol oxidation was studied systematically using platinum based catalysts in membrane electrode assembly form. The electrolyte medium in these MEAs is acidic. The product of complete oxidation of ethanol, carbon dioxide, was monitored and quantified as a function of different parameters like potential, temperature, concentration, catalyst loading or layer thickness and flow rate of the anolyte. CO₂ current efficiency for ethanol oxidation reaction using Pt/C catalyst was found to increase with increasing temperature of operation. CO₂ current efficiency depends strongly on the concentration of EtOH, decreasing with the increase of the latter. At higher ethanol concentration CO₂ becomes a minority product with acetaldehyde taking the lead. The acetaldehyde yield decreases with decrease in concentration and increase in temperature. Acetaldehyde is a stable intermediate, which is quite active for further oxidation if it can readsorb. But with increasing ethanol concentration, desorbed acetaldehyde molecules apparently find it more difficult to find a Pt site for readsorption and thus oxidizing further. Catalyst loading and thus catalyst layer thickness strongly affects the completeness of EtOH oxidation reaction. With increasing catalyst loading CO₂ current efficiency increases. In this respect the fuel cell behaves as a chemical reactor, where the final product distribution of a particular reaction is determined by the available active area and residence time of the reactant. The increasing catalyst layer thickness will result in increasing residence time of the reactants. Also the increasing catalyst loading gives linearly increasing electrochemically active area. These two factors, namely, active area and residence time, are thus responsible for the increase in CO₂ current efficiency with increasing catalyst loading. The residence time of the reactant in a fuel cell anode compartment can also be varied by changing the anolyte flow rates. As expected, the CO₂ current efficiency was found to decrease with increasing anolyte flow rate as the residence time of reactants in the catalyst layer goes down with increasing flow rate. CO₂ current efficiency decreases with increasing potential >0.6 V for ethanol oxidation. Three catalysts, namely, Pt/C, PtSn(7:3)/C, and PtRu(1:1)/C, were compared for CO₂ current efficiency under similar conditions. In these experiments Pt/C and PtSn/C were found to have higher CO₂ current efficiency unlike the case for PtRu/C catalyst. The PtRu/C catalyst showed very low CO₂ current efficiency, although the faradaic currents and onset potential for PtRu/C catalyst were comparable to PtSn/C. This might be explained by the fact that a high amount of Ru in PtRu/C catalyst lowers C-C bond scission rate and promotes partial oxidation of ethanol to acetic acid, by supplying oxygenated surface species which Ru is known to form at much lower potentials. Of the intermediate products, acetaldehyde and acetic acid, acetaldehyde was found to be quite active for further oxidation, but acetic acid seems to be a final by-product, as it is hard to oxidize any further. The obtained results about CO₂ current efficiency variation in ethanol oxidation with parameters like potential of anodic oxidation, temperature, and concentration, will help in the characterization of the ethanol (or other fuels with C-C bond) oxidation catalysts under real fuel cell conditions. The extent of completeness of ethanol oxidation or CO₂ current efficiency under real fuel cell conditions can be very different from the results obtained in model DEMS. This fact emphasizes the importance of fuel cell DEMS measurements.

Acknowledgments

Financial support for this work, in part by the Sino-German Center in Beijing, contract no. GZ 211 (101/11), and the Deutsche Forschungsgemeinschaft DFG, contract no StI 74/14-1, is gratefully acknowledged.

Technische Universität München assisted in meeting the publication costs of this article.

References

1. H. Hitmi, E. M. Belgsir, J. M. Leger, C. Lamy, and R. O. Lezma, *Electrochim. Acta*, **39**, 407 (1994).
2. N. Fujiwara, K. A. Friedrich, and U. Stimming, *J. Electroanal. Chem.*, **472**, 120 (1999).
3. L. W. H. Leung, S. C. Chang, and M. J. Weaver, *J. Electroanal. Chem. Interfacial Electrochem.*, **266**, 317 (1989).
4. D. J. Tarnowski and C. Korzeniewski, *J. Phys. Chem. B*, **101**, 253 (1997).
5. J. Wang, S. Wasmus, and R. F. Savinell, *J. Electrochem. Soc.*, **142**, 4218 (1995).
6. A. S. Arico, P. Creti, P. L. Antonucci, and V. Antonucci, *Electrochem. Solid-State Lett.*, **1**, 66 (1998).
7. G. A. Camara and T. Iwasita, *J. Electroanal. Chem.*, **578**, 315 (2005).
8. H. Wang, Z. Jusys, and R. J. Behm, *J. Phys. Chem. B*, **108**, 19413 (2004).
9. H. Wang, Z. Jusys, and R. J. Behm, *J. Power Sources*, **154**, 351 (2006).
10. C. Lamy, E. M. Belgsir, and J. M. Léger, *J. Appl. Electrochem.*, **31**, 799 (2001).
11. C. Lamy, A. Lima, V. Le Rhun, F. Delime, C. Coutanceau, and J.-M. Léger, *J. Power Sources*, **105**, 283 (2002).
12. C. Lamy, S. Rousseau, E. M. Belgsir, C. Coutanceau, and J.-M. Leger, *Electrochim. Acta*, **49**, 3901 (2004).
13. F. Vigier, C. Coutanceau, F. Hahn, E. M. Belgsir, and C. Lamy, *J. Electroanal. Chem.*, **563**, 81 (2004).
14. F. Vigier, C. Coutanceau, A. Perrard, E. M. Belgsir, and C. Lamy, *J. Appl. Electrochem.*, **34**, 439 (2004).
15. S. Rousseau, C. Coutanceau, C. Lamy, and J. M. Leger, *J. Power Sources*, **158**, 18 (2006).
16. T. Seiler, E. R. Savinova, K. A. Friedrich, and U. Stimming, *Electrochim. Acta*, **49**, 3927 (2004).
17. R. Ianniello, V. M. Schmidt, J. L. Rodry'guez, and E. Pastor, *J. Electroanal. Chem.*, **471**, 167 (1999).
18. J. T. Wang, S. Wasmus, and R. F. Savinell, *J. Electrochem. Soc.*, **142**, 4218 (1995).
19. S. Wasmus, J. T. Wang, and R. F. Savinell, *J. Electrochem. Soc.*, **142**, 3825 (1995).
20. H. Wang, T. Loffler, and H. Baltruschat, *J. Appl. Electrochem.*, **31**, 759 (2001).
21. H. A. Gasteiger, N. M. Markovic, and P. N. Ross, *J. Phys. Chem.*, **99**, 8945 (1995).
22. R. B. d. Lima, V. Paganin, T. Iwasita, and W. Vielstich, *Electrochim. Acta*, **49**, 85 (2003).